Chapter 5

Mechanical Characterization of Brain Tissue in Tension

5.1 Introduction

During severe impact conditions, brain tissue experiences compression, tension and shear. Limited experimental data is available for the brain tissue in extension at dynamic strain rates. Over the past three decades, several research groups investigated some of the mechanical properties of brain tissue (Arbogast et al., 1997; Bilston et al., 2001; Brands et al., 2004; Cheng and Bilston, 2007; Darvish and Crandall, 2001; Estes and McElhaney, 1970; Fallenstein et al., 1969; Hrapko et al., 2006; Miller and Chinzei, 1997; Nicolle et al., 2004; Nicolle et al., 2005; Pervin and Chen, 2009; Prange and Margulies, 2002; Rashid et al., 2012b; Shuck and Advani, 1972b; Tamura et al., 2007; Thibault and Margulies, 1998). However, only a limited number of *tensile tests* has been conducted (Miller and Chinzei, 2002; Tamura et al., 2008; Velardi et al., 2006).

For this Chapter, the mechanical properties of porcine brain tissue have been determined by performing tests at 30, 60 and 90/s strain rates up to 30% strain. The loading rates in the present study approximately cover the range of strain rates as revealed during TBI investigations by various research groups (Bain and Meaney, 2000; Bayly et al., 2006; Margulies et al., 1990; Meaney and Thibault, 1990; Morrison et al., 2006; 2003; 2000b; Pfister et al., 2003). To the author's knowledge, no experimental data for brain tissue in tension at these dynamic strain rates is available except Tamura et al., (2008), who performed tests at 0.9, 4.3 and 25/s, where the fastest rate was closest to impact speeds. The challenge with these tests was to attain uniform velocity during the tension phase of the experiments. Therefore a *High Rate Tension Device* (HRTD) was

designed (discussed in section 3.6, Chapter 3) to achieve uniform velocity at dynamic loading velocities during extension of brain tissue. To fully characterize the behavior of brain tissue, material parameters have been determined by fitting of the data to isotropic one-term Ogden, Fung and Gent models as discussed in section 2.2, Chapter 2. Force relaxation tests in tension were also conducted at various strain magnitudes (10% - 60% strain) with an average rise time of 24 ms. Relaxation data was used to estimate time dependent parameters. Numerical simulations were performed in ABAQUS Explicit/6.9 using material parameters from the one-term Ogden model. The study presented in this chapter may provide new insight into the behavior of brain tissue under dynamic impact conditions, which would assist in developing effective brain injury criteria and adopting efficient countermeasures against TBI.

5.2 Specimen Mounting and Bonding Procedure

The specimen preparation procedure is discussed in section 3.5, Chapter 3 and the experimental setup (HRTD) used to perform tension tests is discussed in section 3.6, Chapter 3. The surfaces of the platens of HRTD were first covered with a masking tape substrate to which a thin layer of surgical glue (Cyanoacrylate, Low-viscosity Z105880–1EA, Sigma-Aldrich) was applied. The prepared cylindrical specimen of tissue was then placed on the lower platen. The top platen, which was attached to the 5 N load cell, was then lowered slowly so as to just touch the top surface of the specimen. One minute settling time was sufficient to ensure proper adhesion of the specimen to the top and lower platens. This procedure provided excellent attachment of the tissue to the platens. A calibrating metal disk of 10.0 mm thickness was also used to confirm the required distance between the platens before the start of experimentation. During tensile tests, excellent bonding was achieved (no slip boundary condition) at the brain/ platen interface due to the application of a thin layer of surgical glue (Cyanoacrylate, Low-viscosity Z105880–1EA, Sigma-Aldrich), as shown in Figure 5.1. However, due to no slip boundary conditions,

localized inhomogeneous deformation of the brain tissue was also observed at the edges of the brain/platen interface. A high speed camera was used to monitor and record all tension tests. The images were used to confirm proper adhesion of brain tissue to the platens during the extension phase.

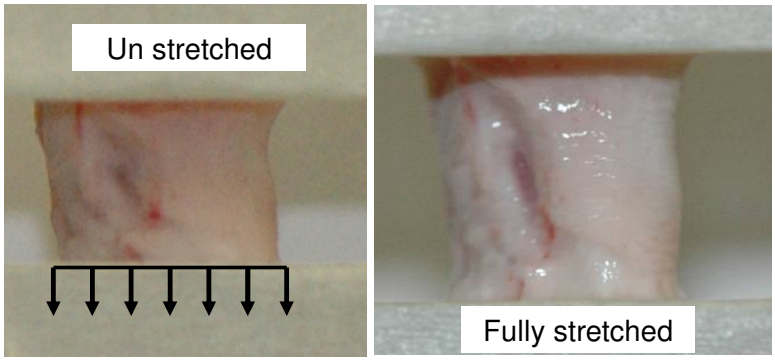

Figure 5.1. Cylindrical brain specimen (10.0 ± 0.1 mm) fully stretched to achieve 30% strain. Arrows indicate downward movement of the lower platen producing stretch in the brain tissue at a specific strain rate.

5.3 Tension Tests

Tension tests were performed up to 30% strain. The velocity of the platen producing extension in the brain tissue was adjusted to 300, 600 and 900 mm/s to attain approximate strain rates of 30, 60 and 90/s, respectively. Four cylindrical specimens containing mixed white and gray matter were extracted from the coronal plane (see Figure 3.1, Chapter 3) from each brain (40 specimens from 10 brains). The attainment of uniform velocity was also confirmed during the calibration process. No preconditioning was performed due to the extreme delicacy and tackiness of brain tissue. All tests were conducted at a room temperature ~ 22^{o} C. A visible contraction of the cylindrical samples occurred immediately after they were removed from the brains, revealing the presence of residual stresses *in-vivo*. When measuring the dimensions of the specimens, it was noted that the nominal dimensions were reached after a few minutes; it was at this stage that testing commenced.

5.4 Force Relaxation in Tension

A separate set of force relaxation tests in tension was performed on cylindrical specimens (10.0 ± 0.1 mm thick and 15.0 ± 0.1 mm diameter). Here, 64 specimens were extracted from 8 brains (4 samples from each cerebral hemisphere) according to the procedure discussed in section 3.5, Chapter 3. Ten force relaxation tests were performed at each of 10%, 20%, 30%, 40%, 50% and 60% strain in order to investigate the response of brain tissue to a step-like strain at variable strain magnitudes. The specimens were stretched at various loading levels (300 – 700 mm/s) and held at the same position while measuring the relaxation force. The average rise time measured from the force relaxation experiments was approximately 24 milliseconds (ms). Force vs. time data was recorded for up to 1.6 s. Force relaxation experiments at dynamic strain rates are very important for the determination of time dependent parameters such as τ_k, the characteristic relaxation times, and g_k, the relaxation coefficients. These are required to simulate impact conditions related to TBI. These parameters can then be used directly in a suitable constitutive model for the determination of stress, taking into account the strain rate dependency of the material.

5.5 Results

5.5.1 Tensile Experiments

Ten tensile tests on cylindrical specimens were performed at each strain rate of 30, 60 and 90/s up to 30% strain in order to analyze experimental repeatability and behavior of tissue at a particular loading velocity, as shown in Figure 5.2. Force (N) and displacement (mm) data measured directly through the four channel data acquisition system (Handyscope, HS4) at a sampling frequency of 10 kHz was converted to engineering stress (kPa) – time (s) for each strain rate. It was observed that the tissue stiffness increases with the increase in loading velocity, indicating the strong stress – strain rate dependence of brain tissue.

The maximum engineering stress at 30% strain at strain rates of 30, 60 and 90/s are 3.1 ± 0.49 kPa, 4.3 ± 0.86 kPa, 6.5 ± 0.76 kPa (mean ± SD), respectively.

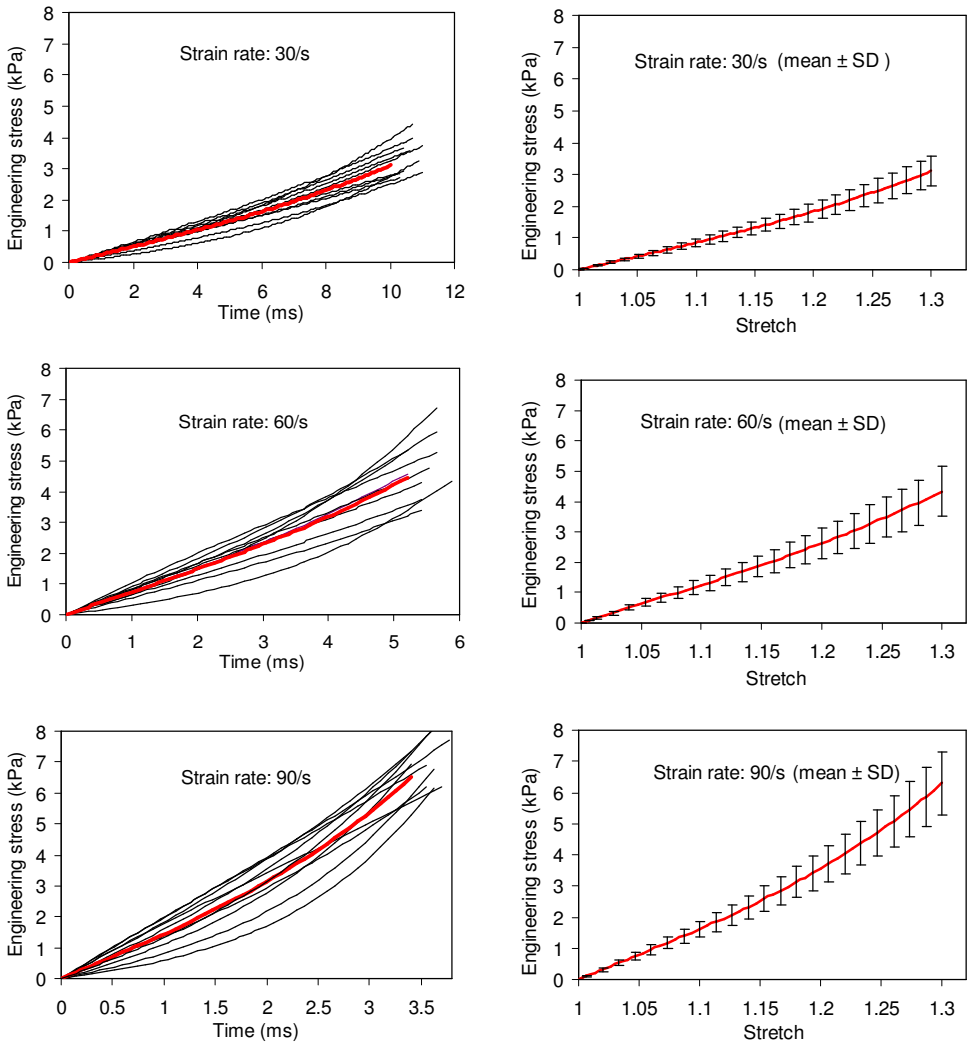

Figure 5.2. Tensile tests performed on porcine brain tissue up to 30% strain at loading velocity of 300 mm/s (strain rate: 30/s), 600 mm/s (strain rate: 60/s) and 900 mm/s (strain rate: 90/s)

5.5.2 Fitting of Constitutive Models

The average engineering stress – stretch curves at each loading rate as shown in Figure 5.2 were used for fitting to hyperelastic isotropic constitutive models (Fung, Gent and Ogden models) already discussed in section 2.2, Chapter 2. Curve fitting was performed by using *lsqcurvefit.m* function available in MATLAB. Excellent fit is achieved for all models (coefficient of

determination: $0.9980 < R^2 \leq 0.9999$) and the resulting theoretical curves are indistinguishable from each another as shown in Figure 5.3. The material parameters were derived after fitting strain energy functions to each experimental engineering stress – stretch profile shown in Figure 5.2. The mean and SD were calculated for all the material parameters. All best fit material parameters (μ, α, b, J_m) derived at each strain rate are summarized in Table 5.1.

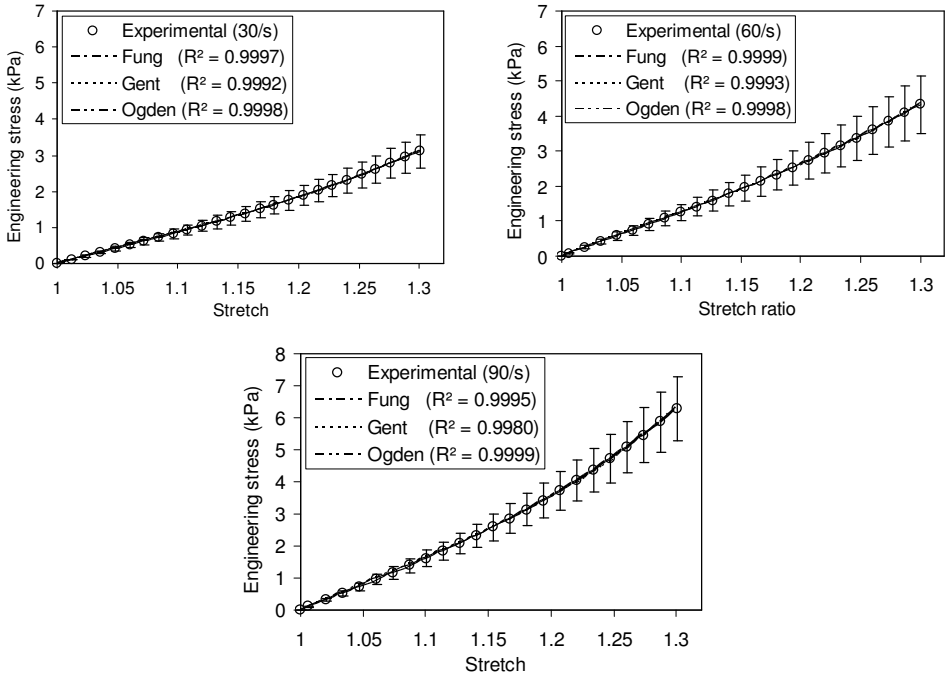

Figure 5.3. Fitting of constitutive models to average experimental data

Table 5.1 – Material parameters derived after fitting of models to experimental data (all μ are in Pa (mean ± SD) and $\mu > 0$)

(1/s)	Fung model		Gent model		Ogden model	
	μ	b	μ	J_m	μ	α
30	3047 ± 643.0	1.68 ±0.88	3114 ± 611.2	0.86 ±0.32	2780 ± 657.4	6.0 ±1.72
	R^2 = 0.9997 ± 0.0002		R^2 = 0.9991 ± 0.0012		R^2 = 0.9997 ± 0.0001	
60	4458 ± 1174.6	1.5 ± 1.0	4548 ± 1127.4	1.15 ±0.71	4112± 1217.2	5.63±2.06
	R^2 = 0.9998 ± 0.0002		R^2 = 0.9993 ± 0.0009		R^2 = 0.9998 ± 0.0001	
90	5739 ± 1913.8	2.19 ± 1.47	5962 ± 1741.3	0.94±0.63	5160 ± 2045.2	6.95±2.85
	R^2 = 0.9995 ± 0.0005		R^2 = 0.9979 ± 0.0026		R^2 = 0.9999 ± 0.0001	

5.5.3 Young's Moduli of Brain Tissue

The Young's moduli at each strain rate were also calculated from the experimental data shown in Figure 5.2. The Young's moduli E_1, E_2 and E_3 calculated from the tangent to the stress – strain curve corresponded to the strain ranges of 0 – 0.1, 0.1 – 0.2 and 0.2 – 0.3, respectively. The estimated Young's moduli at each strain rate are summarized in Table 5.2. There is a consistent rise in moduli for the strain ranges of 0.1 – 0.2 and 0.2 – 0.3. The moduli of brain tissue determined by other research groups were also studied for comparison purpose. Morrison et al. (2003) assumed a Young's modulus, E of 10 kPa in their FE model to predict the strain field in a stretched culture of rat-brain tissue, in which the maximum strain and strain rates were 30% and 50/s respectively. This compares well with the mean Young's modulus, E_1 (strain range: 0 – 0.1) estimated in this study, i.e., 11.68 ± 3.79 (kPa), as indicated in Table 5.2.

Table 5.2 – Young's moduli of brain tissue at each strain rate (mean ± SD)

Strain rate (1/s)	E_1 (kPa)	E_2 (kPa)	E_3 (kPa)
Strain range	0 – 0.1	0.1 – 0.2	0.2 – 0.3
30/s	8.12 ± 2.38	19.2 ± 3.60	29.46 ± 4.28
60/s	10.86 ± 3.74	28.0 ± 6.46	41.05 ± 6.14
90/s	16.08 ± 5.25	35.6 ± 7.74	60.73 ± 7.50
Mean	**11.68 ± 3.79**	**27.6 ± 5.93**	**43.75 ± 5.97**

5.5.4 Force Relaxation Experiments

Force relaxation tests in tension were performed on cylindrical specimens (10.0 ± 0.1 mm thick and 15.0 ± 0.1 mm diameter). Here, 64 specimens were extracted from 8 brains (4 samples from each cerebral hemisphere). Ten force relaxation tests were performed at each strain (10% - 60%) in order to investigate the response of brain tissue to a step-like strain. The specimens were

stretched at various loading levels (300 – 700 mm/s) and then held at the same position while measuring the relaxation force. The average rise time measured from the force relaxation experiments was approximately 24 milliseconds (ms) as shown in Figure 5.4.

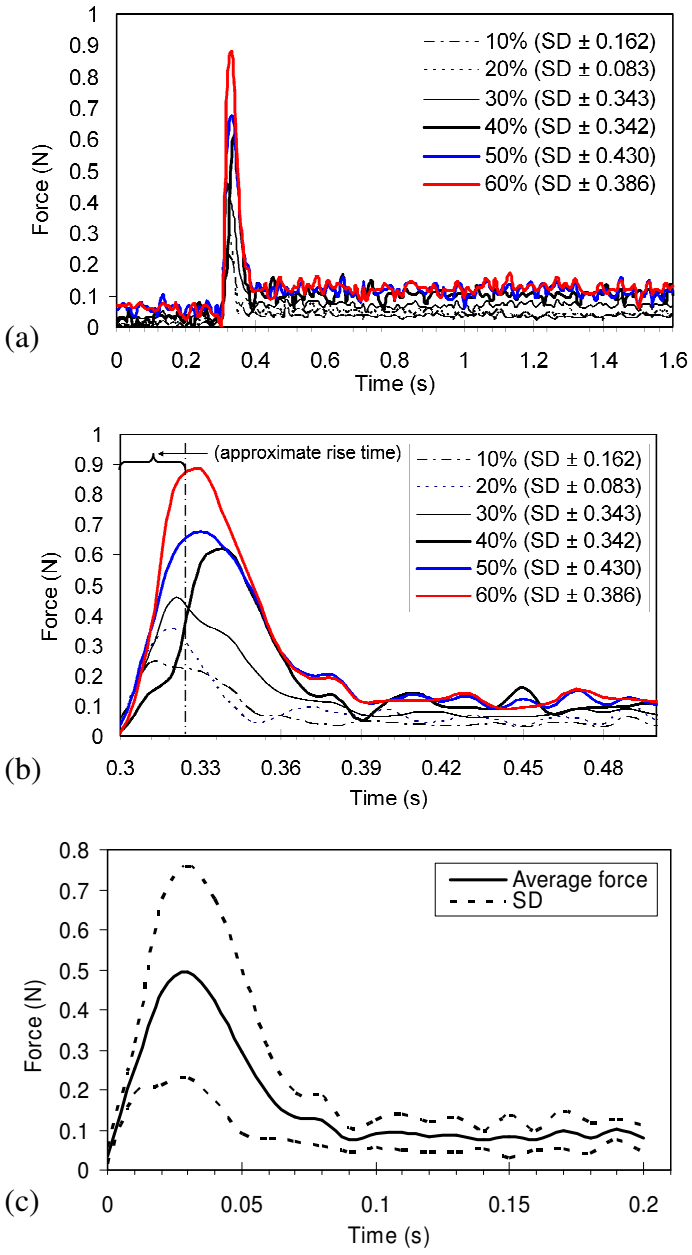

Figure 5.4. (a) Relaxation force (N) at various strain magnitudes (b) the approximate rise time and relaxation force at various strain magnitudes (c) average force and standard deviation, SD (dotted lines)

The peak force relaxed by approximately 83% up to 0.1 s, and then it continuously decreased gradually up to 0.2 s. The dramatic decrease in force reveals the highly viscoelastic nature of brain tissue.

5.5.5 Estimation of Viscoelastic Parameters

The Ogden based hyper-viscoelastic model is discussed in section 2.2, Chapter 2. As a first step, curve fitting of the instantaneous response of a one-term Ogden model (Eq. 2.13, Chapter 2) using experimental data at the maximum loading velocity (strain rate: 90/s) was performed to estimate μ and α. Thereafter, Eq. 2.14 (Chapter 2) was convenient to solve in Matlab 6.9 by using *gradient* and *conv* functions. The *gradient* function was used in order to determine the velocity vector $\frac{d}{d\tau}\left(\lambda^{\alpha-1}-\lambda^{-\frac{\alpha}{2}-1}\right)$ from the experimentally measured displacement, λ, and time, τ. Also, a *conv* function was used to convolve relaxation function (Eq. 2.14) with velocity vector. The coefficients of the relaxation function were optimized using *nlinfit* and *lsqcurvefit* to minimize error between the experimental stress data and Eq. (2.13). The derived Ogden parameters are μ = 5160 Pa and α = 6.95. Similarly, we estimated Prony parameters (g_1 = 0.5837, g_2 = 0.2387, τ_1 = 0.02571 s, τ_2 = 0.0257 s) from a two-term relaxation function using Matlab functions discussed above. These material parameters can be used in ABAQUS software in order to analyze nonlinear viscoelastic behavior of brain tissue.

5.6 Finite Element Analysis

5.6.1 Numerical and Experimental Results

The inhomogeneous deformation of the brain tissue up to 30% strain, particularly near the platen ends, due to no slip boundary conditions was observed during extension of the brain tissue at various loading conditions. Theoretical model developments as discussed in Section 2.2 (Chapter 2) above do not encompass any inhomogeneous deformation of the brain tissue, thus

theoretical deviation from the actual experimentation is expected. Therefore, at this stage, it was necessary to validate the predicted behavior of the theoretical model (using material parameters of one-term Ogden strain energy function, see Table 5.1) of the brain tissue against a numerical model and measured experimental data. Numerical simulations were performed by applying various boundary conditions using ABAQUS 6.9/ Explicit to mimic experimental conditions. A mass density 1040 ± 1 kg/m^3 and hexagonal C3D8R elements were used for the brain part. The bottom surface of the cylindrical specimen (15.0 mm diameter and 10.0 mm thick) was stretched in order to achieve 30% strain, whereas the top surface was constrained in all directions. Before numerical simulations, mesh convergence analysis was carried out by varying mesh density. The mesh was considered converged when there was a negligible change in the numerical solution (0.9%) with further mesh refinement. The total number of elements for the specimen was 9710 with average simulation time of 60 s. An excellent agreement of the average experimental engineering stresses with the numerical engineering stresses (kPa) was achieved as shown in Figure 5.5 (a). Moreover, experimentally measured force (N) was also validated against force determined numerically in a separate set of simulations. Excellent agreement between the average experimental force and the numerical force (N) was achieved, as shown in Figure 5.5 (b).

Figures 5.5 (c) and (d) show deformed states of the cylindrical specimen with stress and force contours, respectively, when stretched to achieve 30% strain. The reaction forces are positive at the moving end and negative at the stationary end of the cylindrical specimen; however the magnitudes of these forces remain the same at both ends of the specimen, as shown in Figure 5.5 (d). Similar simulations were also performed with material parameters estimated at a strain rate of 60 and 90/s. The patterns of stress and force contours were not significantly different from the results shown in Figure 5.5 (c) and (d).

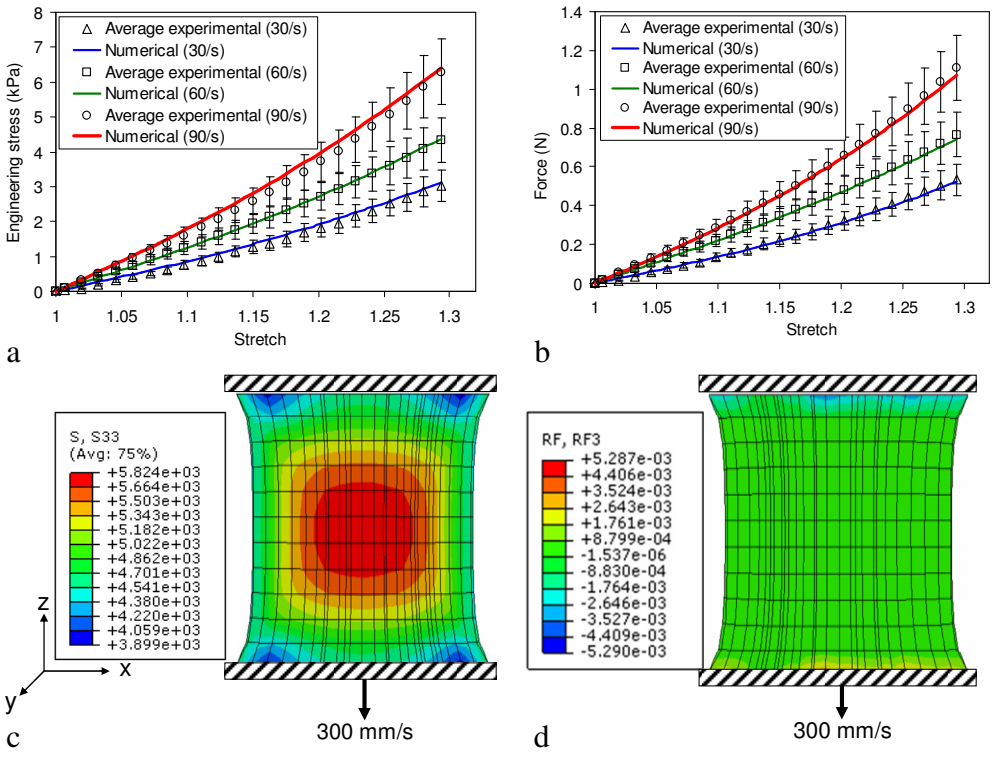

Figure 5.5. Simulations showing numerical stress and reaction force contours (a) agreement of experimental and numerical engineering stresses (kPa) at each strain rate (b) agreement of experimental and numerical forces (N) at each strain rate (c) x sectional view showing stress contours at 30% strain (d) x sectional view showing reaction force (N) contours at 30% strain.

5.6.2 Statistical Analysis and Artificial Strain Energy

The experimental data shown in Figure 5.5 (a) and (b) was analyzed statistically. Based on the one-way ANOVA test, there was no significant difference between the experimental and numerical engineering stresses: p = 0.6379, p = 0.9863 and p = 0.9254 at 30, 60 and 90/s strain rates, respectively, as shown in Figure 5.6 (a). Similarly there was no significant difference between the experimental and numerical forces: p = 0.9190, p = 0.8793 and p = 0.8807 at 30, 60 and 90/s strain rates, respectively, as shown in Figure 5.6 (b). The good agreement between the experimental and numerical results indicates that a one-term Ogden model is appropriate to characterize the behavior of the brain tissue up to 30% strain.

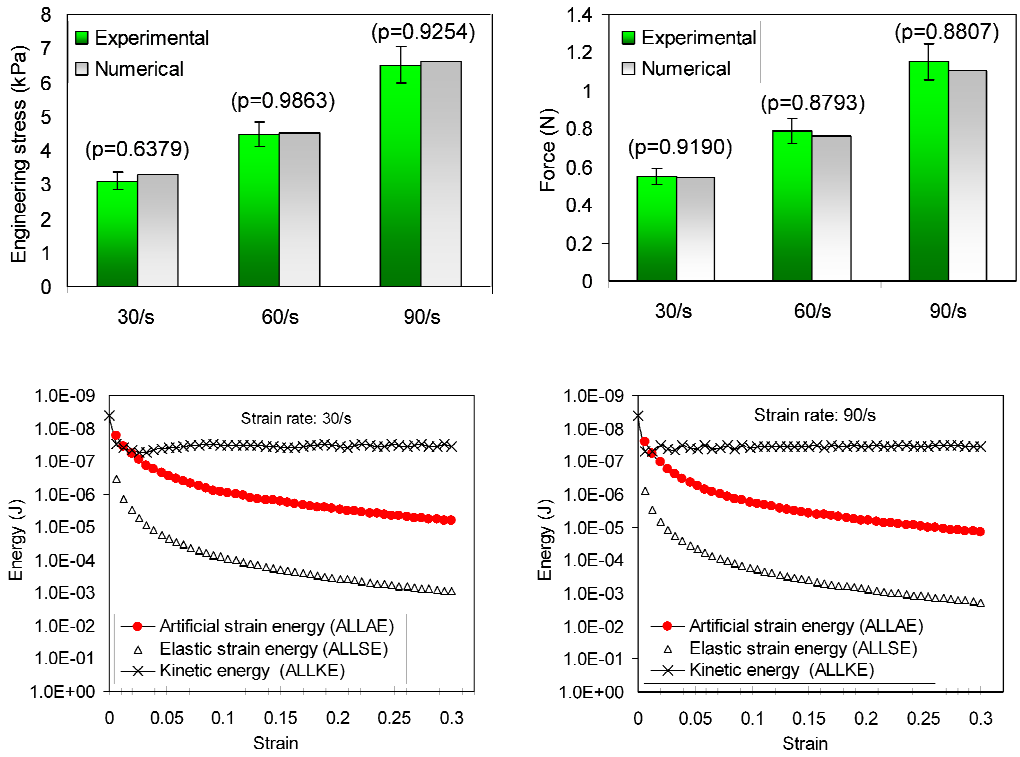

Figure 5.6. There is no significant difference between the numerical and experimental results (engineering stress (kPa) and Force (N)) based on one way ANOVA tests. The accumulated artificial strain energy (ALLAE) as a percentage of the total strain energy is significantly less for the simulations at 30 and 90/s.

The *accumulated artificial strain energy* (ALLAE), used to control *hourglass deformation* during numerical simulations, was also analyzed. It was observed that ALLAE for the whole model as a percentage of the total strain energy was 0.74%, 0.85% and 0.75% for the numerical simulations performed at 30, 60 and 90/s strain rates, respectively as shown in Figure 5.6 (c) and (d). The low percentage of artificial strain energy ($\leq 0.85\%$) observed during the simulations indicates that hourglassing is not a problem; however, this percentage can be reduced further using two-dimensional numerical models.

5.7 Discussion

The characterization of brain tissue in tension at high strain rates is crucial in understanding the mechanism of TBI under impact conditions. On a microscopic scale, the brain is made up of billions of cells that interconnect and

communicate (Nicolle et al., 2004). One of the most pervasive types of injury following even a minor trauma is damage to the nerve cell's axon through shearing during DAI. Several studies have been conducted to determine the range of strain and strain rates associated with DAI. Bain and Meaney (2000) investigated *in vivo*, tissue-level, mechanical thresholds for axonal injury by developing a correlation between the strains experienced in the guinea pig optic nerve and morphological and functional injury. The threshold strains predicted for injury ranged from 0.13 – 0.34. Similarly, Pfister et al., (2003) developed a uniaxial stretching device to study axonal injury and neural cell death by applying strains within the range of 20%–70% and strain rates within the range of 20 – 90/s to create mild to severe axonal injuries. Bayly et al., (2006) carried out *in vivo* rapid indentation of rat brain to determine strain fields using harmonic phase analysis and tagged MR images. Values of maximum principal strains > 0.20 and strain rates > 40/s were observed in several animals exposed to 2mm impacts of 21 ms duration. Studies conducted by Morrison et al., (2006; 2003; 2000b) also suggested that the brain cells are significantly damaged at strains > 0.10 and strain rates > 10/s.

In this research, the properties of porcine brain tissue in extension have been determined up to 30% strain at strain rates of 30, 60 and 90/s by using a custom-designed HRTD which are sufficiently high to cause DAI. The HRTD is specifically designed and calibrated for uniform velocity during the extension phase of brain tissue at strain rates ≤ 90/s. Force relaxation experiments in tension were also conducted at various strain magnitudes (10% - 60% strain) with an approximate rise time of 24 ms. The time dependent Prony parameters can be utilized for a hyperviscoelastic analysis of brain tissue under impact conditions. An excellent agreement between the experimental engineering stresses and numerical engineering stresses indicates that a one-term Ogden model is appropriate to model soft biological tissues in tension up to 30% strain.

Miller and Chinzei (2002) performed tensile tests at room temperature (~ 22^{o} C) on cylindrical specimens of porcine brain tissue (diameter ~ 30 mm; height ~ 10 mm). The specimens were attached using surgical glue. Tamura et al. (2008)

also performed tensile tests at similar temperatures (25 – 28^{o} C) on cylindrical specimens of porcine brain tissue (diameter ~ 14.2 mm; height ~ 14.4 mm), although they used a quench–freeze method to attach their specimens. The comparison of initial elastic moduli, *E* (Pa) at comparable strain rates is presented in Table 5.3.

Table 5.3 Comparison of initial elastic moduli, *E* at strain range (0 - 10%)

Reference	Strain rates: 1/s	*E* (Pa)
Miller and Chinzei (2002)	0.0064, 0.64	530 at 0.64/s
Tamura et al. (2008)	0.9, 4.3, 25	4200 at 0.9/s 18600 at 25/s
Present study	30, 60, 90	8120 at 30/s

It is clearly observed that the elastic modulus at a strain rate of 0.9/s (Tamura et al. (2008)) is approximately 8 times higher than that measured at 0.64/s strain rate (Miller and Chinzei (2002)). Moreover, elastic modulus at a strain rate of 25/s (Tamura et al. (2008)) is approximately 2.3 time higher than at 30/s strain rate (present study). It is possible that the stiffer moduli measured by Tamura et al. (2008) were a consequence of their brain specimens having been frozen for 1 h at –20^{o} C prior to coring out. Such freezing processes usually change the mechanical properties of brain tissue.

In this study, average mechanical properties of brain tissue (mixed white and gray matter) were determined, however, these results are still useful in modelling the approximate behaviour of brain tissue. The average mechanical properties were also determined by Miller and Chinzei (1997; 2002). In previous studies, it was observed that the anatomical origin or location as well as the direction of excision of samples (superior – inferior and medial – lateral direction), had no significant effect on the results (Tamura et al., 2007) and similar observations were also reported by Donnelly and Medige (1997). Based on the research conducted by Prange and Margulies (2002), by using samples of size 55 mm x 10 mm and 1 mm thick, the gray matter showed no difference

between the two orthogonal directions whereas the white matter showed significantly different behaviour.

5.7.1 Comparison of *In vitro* and *In vivo* Results

It is interesting to compare shear moduli obtained from *in vitro* tension tests based on experimental data shown in Figure 5.2 with *in vivo* MRE test protocols. The Young's moduli E_1 at different strain rates (30, 60 and 90/s) were calculated from the stress – strain curves corresponding to the strain range of 0 – 0.1 (see Table 5.2). The shear moduli, G (kPa) were calculated from the Young's moduli; however, initial shear moduli calculated from the one-term Ogden model also confirm same values as shown in Table 5.1. An interesting comparison of shear moduli between the *in vitro* (unconfined compression tests from Chapter 4 and tension tests) and *in vivo* (MRE results from literature) test protocols is shown in Figure 5.7

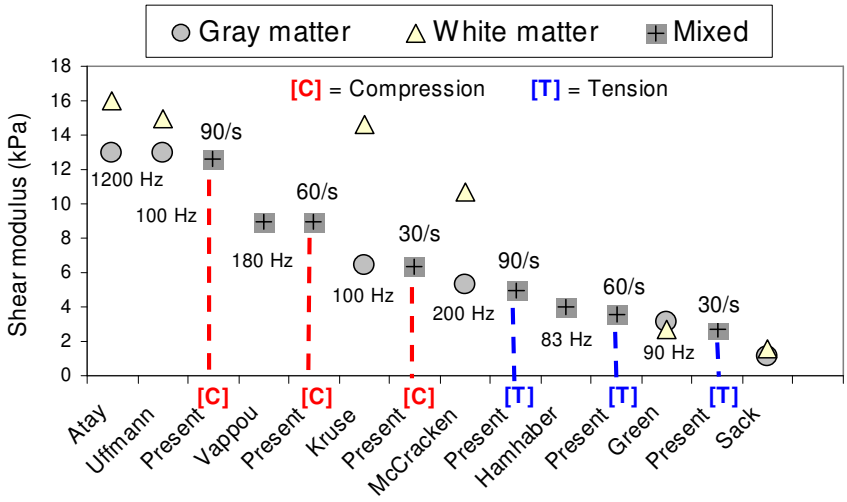

Figure 5.7 – Comparison of shear moduli (kPa) between *in vitro* unconfined compression and tension tests (present research) with the *in vivo* MRE results available in literature.

***In vivo* MRE tests**
Atay et al.(2008) – Mouse
Uffmann et al. (2004) – Human
Vappou et al. (2008) – Rat
Kruse et al. (2007) – Human
McCracken et al. (2005) – Human
Hamhaber et al. (2007)– Human
Green et al. (2008)– Human
Sack et al. (2008) – Human

The shear moduli from tension tests (~ 3.0 – 5.0 kPa) between the strain rates (30 – 90/s) are in agreement with the *in vivo* MRE results available in literature. A reasonable agreement between the shear moduli of human (McCracken et al., 2005) and porcine brain tissue (present study) is obtained at 90/s strain rate as clearly depicted in Figure 5.7. Similarly, a reasonable agreement is achieved between the human (Green et al., 2008; Hamhaber et al., 2007) and porcine brain tissues (present study) at 60 and 30/s strain rates, as shown in Figure 5.7. The comparison of shear moduli from unconfined compression tests at variable strain rates is carried out in Section 4.6.1, Chapter 4.